https://doi.org/10.5194/egusphere-2023-2999
Preprint. Discussion started: 15 January 2024

Variation of atmospheric ^{137}Cs and possible carriers in aerosol samples obtained in Namie in a heavily contaminated area of Fukushima prefecture in 2019

Huihui Li[1], Peng Tang[1]*, Kazuyuki Kita[2]*

1. School of Chemical Engineering, Sichuan University of Science and Engineering, Zigong, Sichuan, 643000, China.

2. Graduate School of Science and Engineering, Ibaraki University, 2-1-1 Bunkyo, Mito, Ibaraki, 310-8512, Japan.

*Correspondence: tpdzyyx@163.com; kazuyuki.kita.iu@vc.ibaraki.ac.jp

Abstract

A lot of radionuclides were released into the environment from Fukushima Daiichi Nuclear Power Plant (FDNPP) accident on March 11, 2011. Because of the long half-life (30.12 years) and high-concentration deposition about ^{137}Cs, the study regarding on the distribution of ^{137}Cs in aerosol samples and the understanding carriers of ^{137}Cs became a hot topic in the recent decade. However, even nine years after FDNPP accident, the explanation for the fluctuations of ^{137}Cs and their carriers in the atmosphere remains elusive. In this study, a small fluctuation within 0.0002 Bqm^{-3} from January to April and a slightly higher level of atmospheric ^{137}Cs from May to September was still observed in the aerosol samples obtained in Namie in a heavily contaminated area of Fukushima prefecture in 2019. Therefore, new observations, obtaining by fluorescent upright microscope and scanning electron microscopes (SEM) equipped with an energy dispersive X-ray spectrometer (EDS), quantitatively demonstrated that the carriers of ^{137}Cs were the combination of C-particles and Al-particles (Al-particles was dominated with the percentage of 68%) in early May; meanwhile the predominate carriers of ^{137}Cs were carbonaceous particles with the average

https://doi.org/10.5194/egusphere-2023-2999
Preprint. Discussion started: 15 January 2024

percentage of 88% in late May and September. Significantly, small particles (less than 2 μm) and medium particles (2-8 μm) of carbonaceous particles had a higher level in the aerosol samples of May and September. Specially, little particles (less than 1 μm), bacteria (1-1.8 μm), and spores (1.8-10 μm) had a linear relationship with the distribution of atmospheric ^{137}Cs in the aerosol samples of September. In addition, the temperature and the precipitation were the main impact factors on the distribution of ^{137}Cs and its carriers.

1 Introduction

1.1 The Fukushima Daiichi Nuclear Power Plant accident

The Fukushima Daiichi Nuclear Power Plant (hereinafter referred to as FDNPP, 37°25′ N, 141°02′ E, which is located on the north-eastern Pacific Ocean coast of Honshu, about 200 km far from north-east of Tokyo) was one of the nuclear power plants of the Tokyo Electric Power Holding Company (TEPCO). At 14:46 on March 11, 2011, a large-scale earthquake (also named as the Great East Japan Earthquake) with a magnitude of 9.0 occurred in the Tohoku region (Herp, 2021). At the moment of the disaster, Units 1 to 3 were normally operating, and Units 4 to 6 were shut down in the scheduled maintenance plan (Tepco, 2011a). The shaking caused by the earthquake and the following disaster of flooding caused by the tsunami resulted in the loss of the electricity of FDNPP, which was needed to run and cool the reactors and spent-fuel-pools normally (Tepco, 2011b). Therefore, a large amount of hydrogen gases was generated by the reaction of uncontrollable residual heat with metal in the units. Although the venting and water-injecting operations were performed in Units 1-3, the hydrogen explosions were not avoided in Unit 1 and Unit 3. Thus, a great many of the radionuclides were released into the atmosphere and deposited on the land and into the pacific ocean (Iaea, 2015).

1.2 Deposition and distribution of ^{137}Cs

There were various radionuclides released into the atmosphere and deposited in the

https://doi.org/10.5194/egusphere-2023-2999
Preprint. Discussion started: 15 January 2024

terrestrial and oceanic environment, which could cause health and environmental pollution, such as contamination problems of soil surfaces, water, agricultural products, and animals by-products, etc. The main radioactive radionuclides were iodine 131 (^{131}I), cesium 134 (^{134}Cs), cesium 137 (^{137}Cs), and xenon 133 (^{133}Xe). As shown in Table 1, the estimated amount of radionuclides released from the FDNPP accident were published by JAEA on April 12, 2011, and NISA on May 12, 2011, respectively (Ohara et al., 2011). Especially, ^{137}Cs has a longer half-life of approximately 30 years, which has attracted much more attention of researchers than other short half-life radionuclides, for example, ^{131}I and ^{133}Xe (which has a short half-life of 8 days and 5 days, respectively) (Christoudias and Lelieveld, 2013). Additionally, the physicochemical properties of ^{137}Cs are similar to potassium. Therefore, the soluble ^{137}Cs was readily absorbed by animals and plants. When ^{137}Cs was entered into the body of animals, it was mainly retained in bone and muscle tissue (Sato et al., 2016). Thus, it is particularly significant to conduct the long-term monitoring and analysis of ^{137}Cs for understanding the fate of ^{137}Cs in the aerosol samples.

Table 1. Radionuclides released from FDNPP accident modified from report of Ohara et al., 2011.

Radionuclide	**Half-life**	**Released amount (Bq)**	
		Japan Atomic Energy Agency (JAEA) 2011/5/12	Nuclear and Industrial Safety Agency (NISA) 2011/4/12
^{131}I	8.040 ± 0.001 days	1.5×10^{17}	1.6×10^{17}
^{132}I	2.30 ± 0.03 hours	—	4.7×10^{14}
^{133}I	20.8 ± 0.2 hours	—	6.8×10^{14}
^{134}Cs	2.062 ± 0.005 years	—	1.8×10^{16}
^{137}Cs	30.17 ± 0.05 years	1.3×10^{16}	1.5×10^{16}
^{106}Ru	368.0 ± 1.6 days	—	2.1×10^{9}
^{129m}Te	33.61 days	—	3.3×10^{15}
^{132}Te	78.2 ± 0.8 hours	—	7.6×10^{14}
^{144}Ce	284.4 ± 0.3 days	—	1.1×10^{13}
^{133}Xe	5.25 ± 0.02 days	—	1.1×10^{19}

https://doi.org/10.5194/egusphere-2023-2999
Preprint. Discussion started: 15 January 2024

1.3 Resuspension of radiocesium

In the report (Onda et al., 2020), there were about 2.7 PBq of ^{137}Cs deposited on the ground, and 60%-67% of them were deposited in the forest. These deposited ^{137}Cs and their carriers were readily the secondary contamination sources. Specifically, in the report (Hirose, 2013), the monthly deposition speed of ^{137}Cs decreased with an apparent half-life of 11-14 days during the period of March-June 2011. Also, the second peak of monthly ^{137}Cs deposition was observed in February-April 2012, which may be ascribed to the resuspension of ^{137}Cs-bearing-particle (CsMPs) (Tang et al., 2022). In addition, most of FDNPP-deriving ^{137}Cs deposited on the topsoil, which remained in the soil surface layer as a potential secondary source of atmospheric ^{137}Cs (Hirose, 2020). The resuspension process of radiocesium could be defined as the redistribution of deposited radioactive cesium into the atmosphere by wind or anthropogenic processes (Igarashi et al., 2003; Igarashi, 2009; Kajino et al., 2016). For bare soil surfaces and forest ecosystems, the respective resuspension rates of ^{137}Cs were estimated as 1×10^{-6} day^{-1} and 2×10^{-6} day^{-1}, which reported by Kajino et al. (Kajino et al., 2016), and revealed a seasonal change that the high level of ^{137}Cs could be observed in warm seasons and the low could be obtained in cold seasons. Also, the resuspension of ^{137}Cs may be derived from the decontamination process in heavily contaminated areas (Steinhauser et al., 2015). However, based on above-mentioned studies, the resuspension of radiocesium and the carriers in the atmosphere has not been fully or accurately understood. Even nine years after FDNPP accident, it was still found a small fluctuation within 0.0002 Bqm^{-3} from January to April and a slightly higher level of atmospheric ^{137}Cs from May to September in the aerosol samples obtained in Namie in a heavily contaminated area of Fukushima prefecture in 2019. This work, for the first time, quantitively demonstrated that the carriers of ^{137}Cs in early May were the combination of C-particles and Al-particles (Al-particles was dominated with the percentage of 68%);

https://doi.org/10.5194/egusphere-2023-2999
Preprint. Discussion started: 15 January 2024

meanwhile the predominate carriers of ^{137}Cs in late May and September were carbonaceous particles with the average percentage of 88%. In addition, the effect of weather conditions (precipitation, air temperature, relative humidity, wind speed, and gust wind speed) on the concentration of ^{137}Cs and their carriers was also discussed. Obviously, the temperature and the precipitation were the main impact factors on the distribution of ^{137}Cs and its carriers.

2 Experimental sections

2.1 Sampling site

The sampling site was a school ground (37°33'44"N, 140°46'07"E, about 30 km far from FDNPP) located in Namie in a heavily contaminated area of Fukushima Prefecture, as shown in Figure 1. It was surrounded by forests, mainly dominated by deciduous forest. Due to the heavy contamination, residents have been evacuated from these contaminated areas. Therefore, the sampling site was free of residential activities, except for decontamination activities and regular research monitoring. As shown in Figure 1, this research site was located at the boundary of the most contaminated area, about 1 MBqm^{-2}.

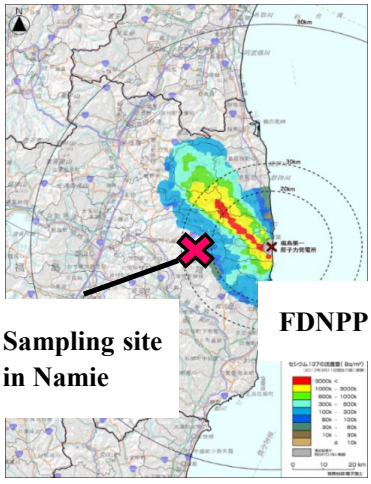

Figure 1. Distribution of deposited ^{137}Cs obtained from the Ministry of Education, Culture, Sports, Science and Technology (MEXT) converted on March 11, 2013 (Mext, 2013), also the sampling site was marked

https://doi.org/10.5194/egusphere-2023-2999
Preprint. Discussion started: 15 January 2024

in a red cross.

Table 2. The information of samples in May and September 2019 giving the name and the sampling time.

2.2 Sampling

Sample name	Starting time		Ending time	
	Year/Month/Day	a.m./p.m.	Year/Month/Day	a.m./p.m.
NHVA-20190501-D-Q	2019/4/26	6:00 p.m.	2019/4/27	6:00 a.m.
NHVA-20190501-L-Q	2019/4/30	6:00 p.m.	2019/5/1	6:00 a.m.
NHVA-20190511-G-Q	2019/5/7	6:00 p.m.	2019/5/8	6:00 a.m.
NHVA-20190511-J-Q	2019/5/10	6:00 p.m.	2019/5/11	6:00 a.m.
NHVA-20190523-A-Q	2019/5/11	6:00 p.m.	2019/5/12	6:00 a.m.
NHVA-20190523-J-Q	2019/5/15	6:00 p.m.	2019/5/16	6:00 a.m.
NHVA-20190923-H-Q	2019/9/20	6:00 p.m.	2019/9/21	6:00 a.m.
NHVA-20190923-J-Q	2019/9/21	6:00 p.m.	2019/9/22	6:00 a.m.
NHVA-20190923-L-Q	2019/9/22	6:00 p.m.	2019/9/23	6:00 a.m.
NHVA-20190929-B-Q	2019/9/23	6:00 p.m.	2019/9/24	6:00 a.m.
NHVA-20190929-H-Q	2019/9/26	6:00 p.m.	2019/9/27	6:00 a.m.
NHVA-20190501-G-Q	2019/4/28	6:00 a.m.	2019/4/28	6:00 p.m.
NHVA-20190511-L-Q	2019/5/10	6:00 a.m.	2019/5/10	6:00 p.m.
NHVA-20190523-K-Q	2019/5/12	6:00 a.m.	2019/5/12	6:00 p.m.
NHVA-20190523-I-Q	2019/5/15	6:00 a.m.	2019/5/15	6:00 p.m.
NHVA-20190923-G-Q	2019/9/20	6:00 a.m.	2019/9/20	6:00 p.m.
NHVA-20190923-K-Q	2019/9/22	6:00 a.m.	2019/9/22	6:00 p.m.
NHVA-20190929-K-Q	2019/9/28	6:00 a.m.	2019/9/28	6:00 p.m.

High-volume aerosol samplers (HV-1000R, Sibata, Japan) equipped quartz fiber filter (2500QAT-UP, Pallflex, USA) were used to collect atmospheric aerosol samples. The sampling flow rate was set to 1000 $Lmin^{-1}$, and the sampling period was a short-term of 12 hours. The daytime and nighttime samples were respectively collected in May and September

https://doi.org/10.5194/egusphere-2023-2999
Preprint. Discussion started: 15 January 2024

2019, with day-time sampling from 6:00 a.m. to 6:00 p.m. and night-time sampling from 6:00 p.m. to 6:00 a.m. of the next day, as detailed given in Table 2. The absent samples in late May and early September 2019 were ascribed to the sampling plan and summer vacation. The quartz filter samples collected by HV aerosol samplers in Namie were stored in the laboratory.

2.3 Meteorological monitoring

Regular meteorological monitoring of the sampling location was also carried out, which was located approximately 800 m far from HV aerosol samplers. The pressure (mbar), solar radiation (Wm^{-2}), wind direction (ø), moisture content ($m^{-3}m^{-3}$), precipitation (mm), air temperature (°C), relative moisture (RH, %), wind speed (ms^{-1}), and speed of gust wind (ms^{-1}) were simultaneously measured per minute. The detailed instrumental settings are shown in Table 3.

Table 3. Several instrumental specifications of meteorological monitoring modified from Appendix of Ishizuka et al., 2017.

Monitoring Object	Instrument	Manufacture	Model
Precipitation	Tipping bucket rain gauge	Takeda Keiki Kougyou	TKF-1
Humidity (RH)	Capacitive chip	Vaisala Corp.	HMP155D
Wind speed	Three cups anemometer	R. M. Young	3102
Gust wind speed	Sonic anemometer	R. M. Young	81000
Air temperature	Pt resistance thermometer	Vaisala Corp.	HMP155D
Moisture	ADR sensor	Delta-T Devices Ltd.	Theta probe ML2x

3 Radioactivity measurement and observations of samples

3.1 Radioactivity measurement

The radioactivity of ^{134}Cs, ^{137}Cs was measured at the peak gamma-ray at 605 keV and

https://doi.org/10.5194/egusphere-2023-2999
Preprint. Discussion started: 15 January 2024

662 keV, respectively, using coaxial Ge semiconductor equipped with computerized spectrum analyzer in the Meteorological Research Institute (MRI) and the University of Tsukuba. The atmospheric radioactive concentration of ^{137}Cs was calculated by

$$C_{\text{filter}} = Q_{\text{filter}} / V_{\text{filter}} \quad (1)$$

where C_{filter} (Bqm^{-3}) was the atmospheric radioactive concentration of ^{137}Cs, Q_{filter} (Bq) was the radioactive intensity of ^{137}Cs in quartz fiber measured by coaxial Ge semiconductor, and V_{filter} (m^3) was the volume of the sampling air.

3.2 Microscope observations

Two pieces of Φ33 mm were taken out from the HV aerosol filter sample (8 × 10 inches) for DAPI (4',6-diamidino-2-phenylindole) staining: one piece (a) was obtained in the middle area and the other piece (b) was obtained in the edge area from the same aerosol filter sample. The rest of the aerosol filter sample was sealed and stored for other experiments. Then, one piece of Φ12 mm was taken out from each piece of Φ33 mm for further treatment. Finally, two pieces of Φ12 mm were obtained and the rest of each piece of Φ33 mm was sealed and stored for backup. For all samples, the two pieces of Φ12 mm filters were firstly fixed by formaldehyde solution, and then dried for 2 hours. Formaldehyde solution was used for preserving or fixing tissues or cells due to its functions of embalming, fixing cadavers, disinfection, and bleaching. DAPI for fluorescent staining, because DAPI could penetrate the cell membrane and strongly fix the DNA in the nucleus (Maki et al., 2013). After staining, the samples were rinsed with ultrapure water and dried, in the end, the samples were stored in dark light. For fluorescence observation, the DAPI-stained cells were able to be labeled with blue fluorescence, after excitation by UV light with the wavelength of 360-400 nm, using the fluorescent upright microscope (BS-2040TF, Bio Tools Inc., Gunma, Japan). The dark particles (all particles) could be observed with the reflected-light mode, and the colored particles (carbon-containing particles) could be observed in the fluorescence-mode because

https://doi.org/10.5194/egusphere-2023-2999
Preprint. Discussion started: 15 January 2024

the DAPI-stained particles could be shown blue or yellow fluorescence illuminated by UV light under the fluorescent upright microscope. Five sites of each Φ12 mm sample were used for observations using fluorescent upright microscope. Each site was photographed with a CCD camera in reflected-light mode and in fluorescent-light mode, respectively. Finally, all images were saved for the analysis of the size and morphology of aerosol particles. A total of 10 images were taken for each Φ12 mm sample, and a total of 20 images were taken for each sample collected in our sampling site. The images (the number and Feret's diameter of particles) were analyzed by a free professional software of Image J (Kita et al., 2020). The morphology, the elemental compositions and distribution of the aerosol particles was characterized by a SEM (SU3500, Hitachi High-Technologies Co., Tokyo, Japan) equipped with an EDS (X-max, Horiba Ltd., Kyodo, Japan) in MRI.

4 Results and discussion

4.1 Variations of ^{137}Cs in aerosol filters sampled in 2019

4.1.1 Annual variations of atmospheric ^{137}Cs

The annual variations of ^{137}Cs in the HV aerosol filters sampled in 2019 were shown in Figure 2 (the absent samples were ascribed to the sampling plan and vacations). It could be found a small fluctuation of atmospheric ^{137}Cs within 0.0002 Bqm^{-3} from January to April. It was obvious that a slightly higher level of ^{137}Cs could be observed from May to September. Moreover, it can be obtained the seasonal variation of the atmospheric ^{137}Cs that the level of ^{137}Cs was higher in the warm season (from May to September) and lower in the cold season (from January to April). Significantly, there were two peaks that appeared in May (about 0.00072 Bqm^{-3}) and September (about 0.00052 Bqm^{-3}). These two peaks may be caused by the resuspension of aerosol particles carrying ^{137}Cs, which will be discussed later in detail. Thus, in the following section, variations of atmospheric ^{137}Cs for HV filter samples collected in May and September were mainly discussed.

https://doi.org/10.5194/egusphere-2023-2999
Preprint. Discussion started: 15 January 2024

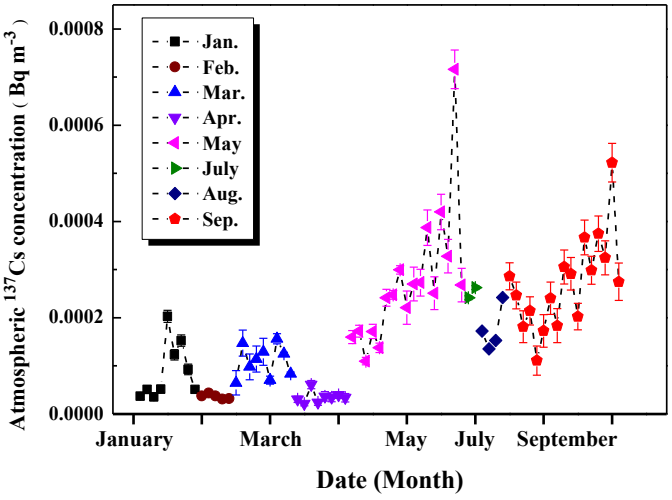

Figure 2. Annual variations of ^{137}Cs in aerosol filters sampled in 2019.

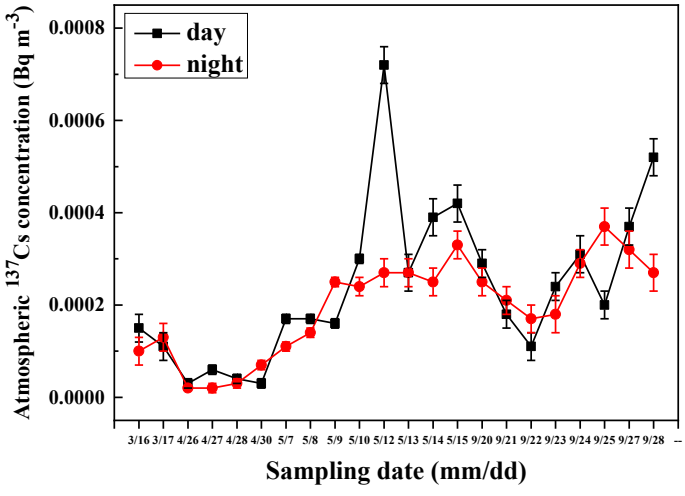

Figure 3. Diurnal variations of ^{137}Cs in the aerosol filters sampled in the day-period/night-period in 2019. The sampling date defined as mm/dd. Blackline represents variations of ^{137}Cs concentration in the day-period. Redline was the variations of the samples obtained in the night-period.

https://doi.org/10.5194/egusphere-2023-2999
Preprint. Discussion started: 15 January 2024

4.1.2 Diurnal variation of ^{137}Cs

The comparison of daytime and nighttime variation of atmospheric ^{137}Cs was shown in Figure 3. There were 22 groups of ^{137}Cs in HV filter samples collected in the day-period and night-period, respectively. Clearly, it can be found that the concentration of ^{137}Cs in the daytime samples were slightly higher than that sampled in the nighttime. Specifically, among the 22 groups of ^{137}Cs, 15 groups had a positive differences in atmospheric ^{137}Cs between daytime and nighttime samples. Also, it can be noticed that the concentrations of ^{137}Cs sampled in the day-period on the 12 May and on 28 September were about 3 times and 2 times higher than that of those samples collected in the night-period, respectively. Especially, the diurnal variations of ^{137}Cs were similar to the seasonal variation of ^{137}Cs as mentioned above in the annual variations of ^{137}Cs. Specifically, the maximum of ^{137}Cs concentration was 0.00072 Bqm^{-3} sampled in a day-period on 12 May and the minimum was 0.00002 Bqm^{-3} sampled in the night-period on 26 April and 27 April. In Autumn (late September), the maximum of ^{137}Cs concentration was 0.00052 Bqm^{-3} sampled a day-period on 28 September, and the minimum was 0.00011 Bqm^{-3} sampled a day-period on 22 September.

4.2 Possible carriers of ^{137}Cs in May and September

4.2.1 Possible carriers of ^{137}Cs for the HV samples collected in May 2019

SEM observations of the HV filter sample (#NHVA2019-0511-J-Q) were shown in Figure 4. Comparative analysis of the observations was shown in Figure 4a in backscattered electrons mode, BSE, and Figure 4b in low-vacuum mode. Clearly, there were some grey-white particles with diameters of 20-35 μm, which could be easily identified as pollen particles. Meanwhile, there were also some small, clear, white, elliptic-shaped particles and they were mapped by EDS, as shown in Figure 4c, 4b, and 4d. Significantly, the several large carbon-containing particles could be pollens as shown in Figure 4c, and some small particles may be organic matters (such as fungal cells and/or debris, sporangia or ascospores or other

https://doi.org/10.5194/egusphere-2023-2999
Preprint. Discussion started: 15 January 2024

microorganisms). In Figure 4d and 4e, it can be found that there were a lot of small aluminum-containing and iron-containing particles, which may be mineral particles or soil dusts. Overall, in Spring, more iron/aluminum-containing mineral particles of 2-5 μm and some scattered pollens and/or organic particles can be observed, indicating that main possible carriers of ^{137}Cs in HV filters collected were the mineral particles.

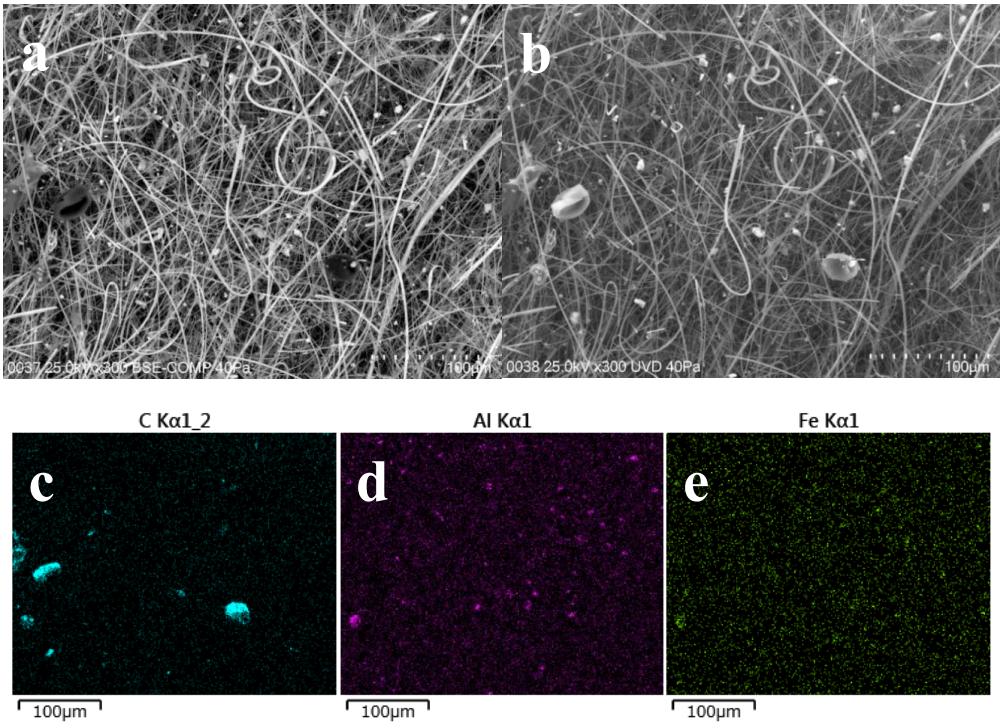

Figure 4. SEM images and elemental distribution maps of the HV filter named #NHVA2019-0511-J-Q: a) SEM image obtained in backscattered electrons mode; b) SEM image got in low-vacuum mode; c) Elemental distribution of carbon; d) Elemental distribution of aluminum; e) Elemental distribution map of iron.

In the typical optical microscopy photograph (Figure 5a) and fluorescent micrograph (Figure 5c) of 4,6-diamidino-2-phenylindole (DAPI) staining particles in the HV filter sample (#NHVA2019-0523-J-Q), it can be found a lot of bioaerosol particles. After treatment

https://doi.org/10.5194/egusphere-2023-2999
Preprint. Discussion started: 15 January 2024

by Image J software, equivalent projected images were used for counting and classifying particles in the reflected-light mode (Figure 5b) and fluorescent-light mode (Figure 5d), respectively. It is easy to distinguish some pollen particles with a size larger than 20 μm (Figure 5a). Based on the fluorescent color and morphology of the lighted particles, the fluorescent aerosol particles could be classified into different bioparticles. Specifically, in Figure 5c, it could be found that the most abundant fluorescent aerosol particles were 1) big elliptic blue particles (diameter >20 μm, indicating pollens or aggregated particles), 2) spindly yellow and blue particles (10 μm < diameter <20 μm, microbial particles of sporangia or ascospores), 3) elliptic yellow and blue particles (diameter <10 μm, identified as bacteria or basidiospore), and 4) white particles indicated other organics.

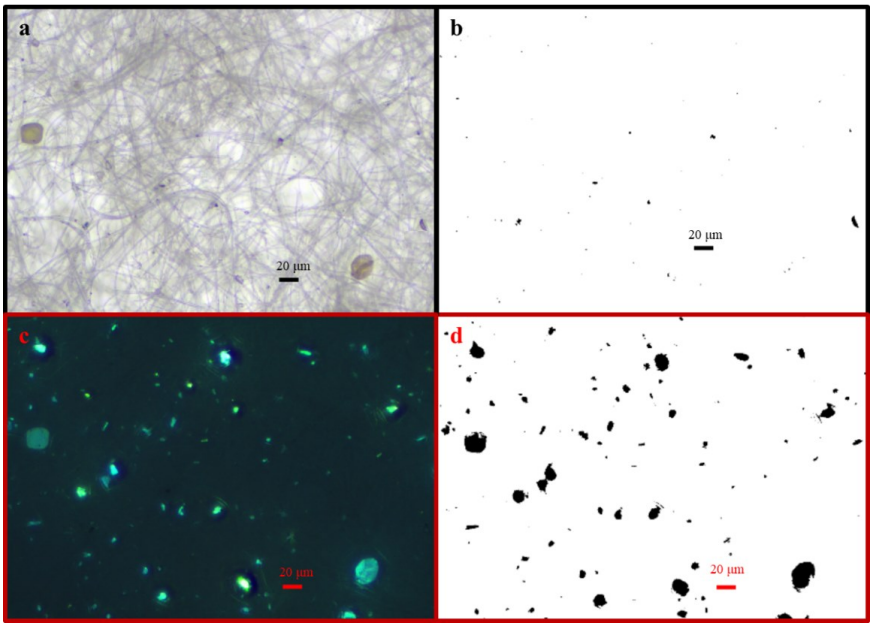

Figure 5. Microscope images (BS-2040TF) and processed equivalent projected images by Image J in the same site of a HV filter sample (#NHVA2019-0523-J-Q) collected in May 2019: (a) microscope image in reflected-light mode; (b) equivalent projected area image of Figure 5a; (c) microscope image in fluorescent-light mode; (d) equivalent projected area image of Figure 5c.

https://doi.org/10.5194/egusphere-2023-2999
Preprint. Discussion started: 15 January 2024

The classifications of fluorescence highlighted particles were consistent with that of the reference (Igarashi et al., 2019b). Additionally, only particles with sizes larger than 0.65 μm were counted in this study. Particularly, it is observed that numerous particles with multiple septa, which were most possible the fungal spores of the phylum Ascomycota. More bioaerosol particles are observed in September than in May (based on the comparation in Figure 5c and 8c). It was possibly due to a seasonal change in the bioaerosol source or rainy weather on the sampling days in September, which has also been discussed in the report of Kita et al. (Kita et al., 2020). As a consequent, after analyzing all particles, large particles (such as ascospores, pollens, fragments, aggregated particles), small particles (such as bacteria), and medium particles (such as basidiospores) could be observed and classified. Therefore, the abovementioned six types of particles were discussed in the following section.

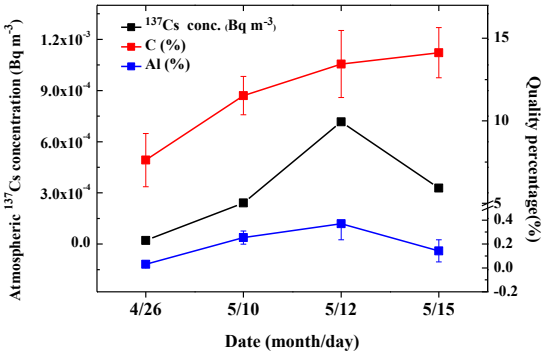

Figure 6. Variation of ^{137}Cs, C% and Al%.

Based on the SEM observations (Figure 4), it could be obtained that many small mineral particles were also found in HV filter samples collected in May. Meanwhile, the optical microscope images (Figure 5) also exhibited many dispersed organic large particles, such as pollen particles. Thus, it was assumed that the carriers of ^{137}Cs in the filter samples collected in May can be alternated during this sampling period, because May was just located in the alternate period of spring and summer. In addition, four HV filter samples collected in May

https://doi.org/10.5194/egusphere-2023-2999
Preprint. Discussion started: 15 January 2024

were analyzed by SEM/EDS for estimating the elemental mass percentage. The variation of ^{137}Cs and elemental mass percentage of Al and C with sampling time were shown in Figure 6. The black points were the concentration of ^{137}Cs, the red and the blue symbol represented the percentage of C and Al, respectively. It was obvious that the variation of ^{137}Cs concentration was consistent with the trend of Al%. Specifically, the gradual increase of ^{137}Cs concentration and Al% was observed from 26 April to 12 May, reaching the peak on 12 May. After 12 May, Al% showed a clear downward trend. In contrast, the variation of C% was always in a slowly increasing trend. There would be a period for ^{137}Cs carrier's transition from mineral particles (aluminum-containing particles) to carbonaceous particles. Therefore, it could be assumed that the mineral particles or soil dusts could be the main carriers of ^{137}Cs in early Spring. On the other hand, the carbon-containing particles may be the dominated carriers of ^{137}Cs in the late Spring, but more data and further discussion are still needed.

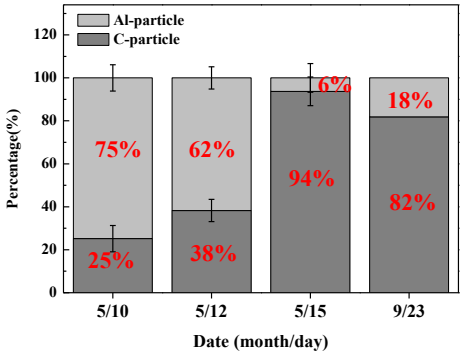

Figure 7. Comparative percentage variations of carbon- and aluminum- containing particles.

In Figure 7, the comparative variation of carbon-containing particles and aluminum-containing particles estimated from SEM-EDS observations was provided. It could be noticed that the percentage of carbon-containing particles gradually increased, on the contrary, the percentage of aluminum-containing particles gradually decreased from 10 May to 15 May, which is consistent with the assumption that the mineral particles or soil dusts

https://doi.org/10.5194/egusphere-2023-2999
Preprint. Discussion started: 15 January 2024

could be the main carriers of ^{137}Cs in early Spring and the carbon-containing particles could be the dominated carriers of ^{137}Cs in the late Spring. Moreover, a close higher-level percentage of carbon-containing particles was found in the samples collected on 15 May and 23 September with the percentage of carbon-containing particles of 92%, and 82%, respectively, which indicated that the main carriers of ^{137}Cs may be carbon-containing particles. This result was consistent with our previous master's research (Kimura, 2019a) that the bio-particles gradually became the dominant carriers of ^{137}Cs. These results were also consistent with the speculation that the mineral particles or soil dusts could be the main carriers of ^{137}Cs in early Spring and the carbon-containing particles could be the gradually dominated carriers of ^{137}Cs in the late Spring.

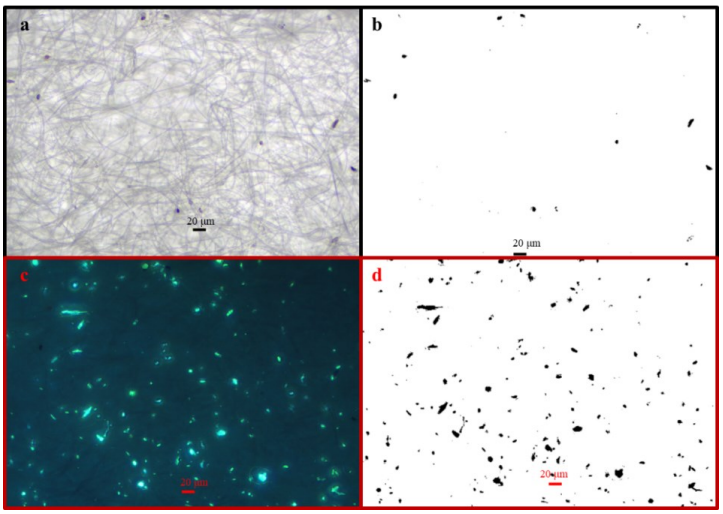

Figure 8. Microscope images (BS-2040TF) and processed equivalent projected images by Image J in the same site of a HV filter sample (# NHVA2019-0923-L-Q) collected in September 2019: (a) microscope image in reflected-light mode; (b) equivalent projected area image of Figure 8a; (c) microscope image in fluorescent-light mode; (d) equivalent projected area image of Figure 8c.

https://doi.org/10.5194/egusphere-2023-2999
Preprint. Discussion started: 15 January 2024

4.2.2 Possible carriers of ^{137}Cs for the HV samples collected in September 2019

As shown in the typical optical microscopy photograph (Figure 8a) and fluorescent micrograph (Figure 8c) of DAPI staining particles in the HV filter sample (#NHVA2019-0923-L-Q), it was easily observed that there were more bio-particles with different morphology and size, which were consistent with report that bio-particles could be the main carriers of ^{137}Cs in autumn (Kimura, 2019b; Igarashi et al., 2019b).

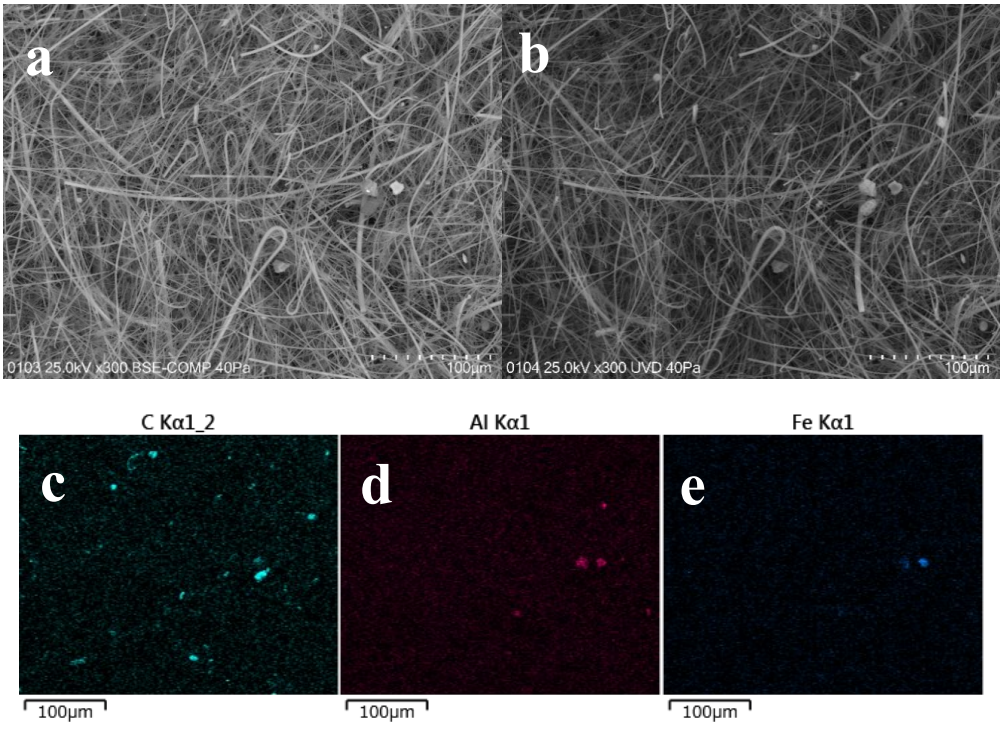

Figure 9. SEM images and elemental distribution maps: a) SEM image obtained by BSE model; b) SEM image got by UVD; c) Compositional map of C; d) Compositional map of Al; e) Compositional map of Fe. Sample name is #NHVA2019-0929-B-Q. The bar is 100 µm.

SEM observations of the HV filter sample (#NHVA2019-0929-B-Q) were shown in Figure 9. Compared with Figure 9c, 9d, and 9e, there were a higher level of carbonaceous

https://doi.org/10.5194/egusphere-2023-2999
Preprint. Discussion started: 15 January 2024

particles and fewer aluminum-containing and iron-containing particles, which indicates carbon-containing particles could be the dominated carriers of ^{137}Cs in September. It was also consistent with the results of microscope observations, as shown in Figure 8.

4.3 Bioaerosol particles and their size distributions

According to the observations of optical, fluorescent microscope, and SEM-EDS, aerosol particles in the aerosol filter samples collected in May and September 2019 were mainly analyzed. Diameter was described as the Feret diameter (along the selection boundary, the longest distance between any two points, also known as maximum caliper), which was obtained from the microscope images using Image J. Figure 10a and 10b were the size distributions of bioaerosol particles in the HV filter samples collected in May 2019. It could be easily noticed that the particles with the diameter (d < 1 μm) were predominant. The second peak represented the particles with a diameter less than 2 um. Similarly, the size distribution of bioaerosol particles in the HV filter samples collected in September 2019 was given in Figure 10c. A wider diameter range of the bioaerosol particles could be found in three peaks (d < 1 μm, d < 2 μm, and d < 8 μm). In addition, bioaerosol particles with a diameter less than 1 μm were also predominant. Quantitatively, from Figure 10a (early May) to Figure 10b (late May), the normalized number of particles had increased nearly 3 times (obtained by the value of first peak), which was consistent with the SEM observations as shown in Figure 7. Similarly, from Figure 10b (late May) to Figure 10c (September), the normalized number of particles had no apparent change. Overall, although the size distribution appeared bimodal or multi-peaked in Figure 10b and 10c, the bioaerosol particles with the diameter (< 2 μm) could be the predominant possible carriers of ^{137}Cs.

https://doi.org/10.5194/egusphere-2023-2999
Preprint. Discussion started: 15 January 2024

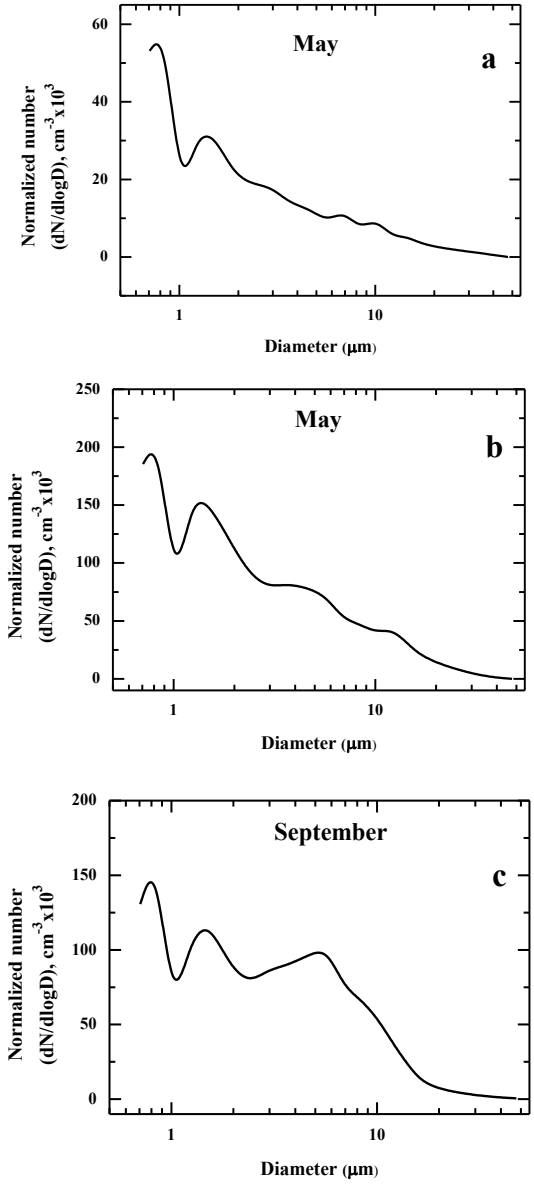

Figure 10. Normalized particle number size distributions of bioaerosol particles in the HV filter samples collected in May (a: # NHVA2019-0501-G-Q, b: # NHVA2019-0523-J-Q) and September (c, # NHVA2019-0923-J-Q) in 2019.

https://doi.org/10.5194/egusphere-2023-2999
Preprint. Discussion started: 15 January 2024

4.4 Relation between aerosol particles and ^{137}Cs

In Figure 11a, the unstained particles represented mainly mineral particles and some bioaerosol particles, which were difficult to stain in the DAPI staining experiment. In Figure 11b, the stained particles referred to mainly bioaerosol particles, which could be observed in blue/yellow/white lighted particles under fluorescent light. The blue points and the red points represented the correlation between the concentration of atmospheric ^{137}Cs and the concentration of aerosol particles, which were respectively estimated from the HV aerosol filter samples collected in May 2019 (there were ten samples, n=10) and in September 2019 (there were eight samples, n=8), respectively. It was obviously found that the unstained particles of mainly mineral particles had a strong positive correlation with the concentration of atmospheric ^{137}Cs both in May and September 2019, as shown in Figure 11a. As mentioned in Figure 7-10, it was consistent with the assumption that the combination of mineral particles and bio-particles could be the main possible carriers of ^{137}Cs in May 2019.

In Figure 11b, the stained particles also had a positive correlation distribution with ^{137}Cs in September 2019, reconfirming that the bioparticles could be predominant carriers of ^{137}Cs (which was also consistent with the results in Figure 8 and 9). In contrast, in May, the ^{137}Cs concentration did not have a good linear relation with concentration of colorless particles, which may be caused by the fact that the combination of mineral particles and bioparticles could be the main carriers of ^{137}Cs in May 2019. Namely, the dominant carriers of ^{137}Cs could be mineral particles in early May and bio-particles in late May (as shown in Figure 5 and 7). It seems to be consistent with other studies (Kinase et al., 2018; Igarashi et al., 2019b) that there were different resuspension mechanisms in May and September. Namely, it was generally believed that there was a much lower concentration of ^{137}Cs, and the main carriers could be mineral particles in the Spring. In Summer and Autumn, there were relatively higher concentration of ^{137}Cs, and the bioaerosol particles could be predominant in the aerosol

https://doi.org/10.5194/egusphere-2023-2999
Preprint. Discussion started: 15 January 2024

particles, which also implied that the bioaerosols were more possible to be the carriers of ^{137}Cs in September (Kita et al., 2020).

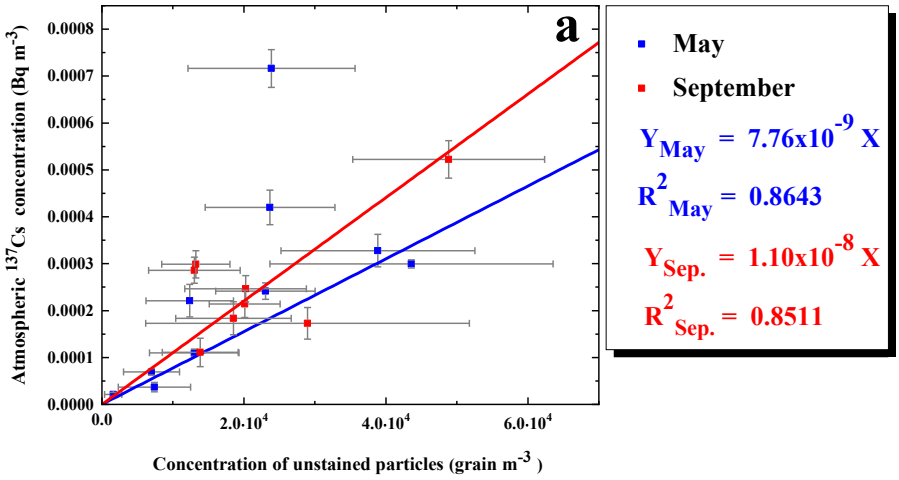

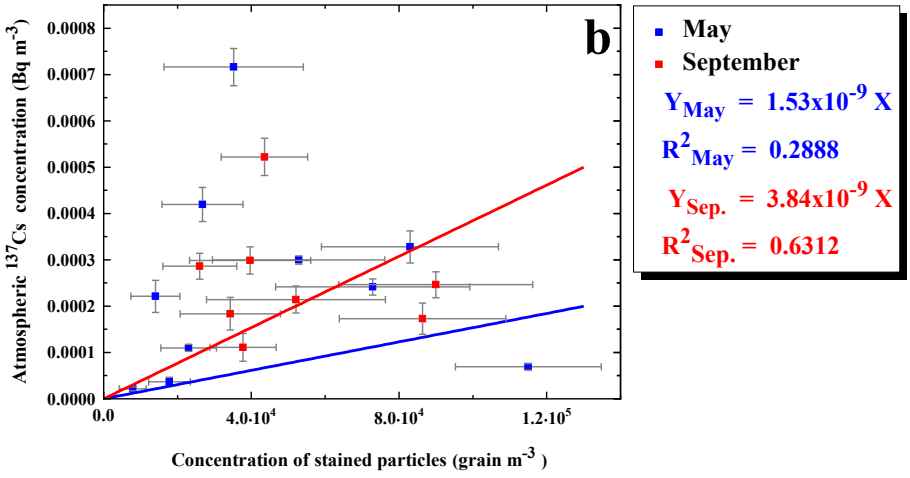

Figure 11. The concentration variations of atmospheric ^{137}Cs with the concentration of aerosol particles, which were respectively estimated from the HV aerosol filter samples collected in May 2019 (there were ten samples, n=10, highlighted in blue points) and in September 2019 (there were eight samples, n=8,

https://doi.org/10.5194/egusphere-2023-2999
Preprint. Discussion started: 15 January 2024

highlighted in red points).

Table 4. Classification of bioaerosol particles based on different sizes. AR (Aspect Ratio) represented the ratio of the major to the minor. The major and the minor were the primary and secondary axises of the best fitting ellipse. Circularity was defined as 4π×(area) / (squared circumference). When the value of circularity was 1, representing the particle that could be regarded as a perfect circle. If the value approached 0, it indicated that the shape of the particle was elongated. When the AR was greater than 4 and the circularity was less than 0.45, the particle was defined as a fragment.

Species	Parameter		Size		References	Appearance Examples
	AR	Circularity	Major	Minor		
Fragment	>4	<0.45				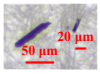
Little particle	<4	>0.45	0.65-1.0μm	0.65-1.0μm		
Bacteria	<4	>0.45	1.0-1.8μm	1.0-1.8μm	Hoorman et al. (2011)	
Basidiospore	<4	>0.45	1.8-10μm	1.8-5μm	Yamamoto et al. (2012)	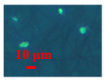
Ascospore	<4	>0.45	10-60μm	5-15μm		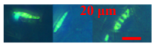
Pollen	<4	>0.7		>15μm	Stanley and Linskins (1974); Kelly et al. (2002)	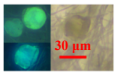
Others						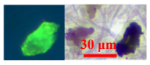

Igarashi et al. reported a strong relationship between carbon-bearing particles and ^{137}Cs concentration (Igarashi et al., 2019b). Also, combining the abovementioned discussion, the main carriers of ^{137}Cs were mineral particles in early May, and the predominant carriers of ^{137}Cs were bioaerosol particles in late May and in September 2019. Therefore, it was necessary to quantify the relation between bioaerosol concentration and ^{137}Cs concentration to estimate the predominant contribution of the specific type of bioaerosol particles to the atmospheric ^{137}Cs. According to the classification, as shown in Table 4, there were several common types of bioaerosol particles (Stanley and Linskens, 2012; Kelly et al., 2002;

https://doi.org/10.5194/egusphere-2023-2999
Preprint. Discussion started: 15 January 2024

Yamamoto et al., 2012; Hoorman, 2011). Then, a multiple linear regression was used to estimate the kinds of bio-particles variated with the dominant carriers of ^{137}Cs, as follows:

$$I = \sum_i a_i * A_i + b_0 \quad (2)$$

Where I (Bq) was the total radioactivity of ^{137}Cs in the HV aerosol filter samples, i was a serial number, i = 1, 2, 3, 4, 5, 6 (little particle, bacteria, spore, ascospore, pollen, fragment) and so on, a_i was the coefficient (Bq μm^{-2}), A_i is the area of the HV filter samples (183.2 mm × 234 mm), and b_0 was residual radioactivity of ^{137}Cs of the HV filter (Bq).

Table 5. Each coefficient in equation (2). a_i was the coefficient of each bioaerosol, referring to the ^{137}Cs radioactivity accumulated in each type of bioaerosols within each HV aerosol filter sample. The statistical analysis was made by regression analysis for 10 samples. Asterisk (∗) indicated a significance level.

a_i	Coefficient value (Bq μm^{-2})	b_0	Residual radioactivity (Bq)
a_1	1.11×10^{-8}	b_0	0.19
a_2	3.08×10^{-8} *		
a_3	9.14×10^{-12}		
a_4	0.00		
a_5	0.00		
a_6	0.00		

In Figure 12, the relationship between each type of bioaerosols and ^{137}Cs was obtained by the multiple linear regression analysis. The black symbol was the measured value of ^{137}Cs obtained from the coaxial Ge semiconductor detector. The red points represented the predicted radioactivity value estimated from equation (2). The other symbols represented the contribution of different bioaerosol particles to the radioactivity of ^{137}Cs.

The distribution of ^{137}Cs for each bioaerosol in aerosol filter samples collected in September 2019 was given in Table 6. As a result of a multivariate analysis (performed by least-squares) under non-negative constraints, the contribution of each species of bioaerosols

https://doi.org/10.5194/egusphere-2023-2999
Preprint. Discussion started: 15 January 2024

to the radioactivity of ^{137}Cs and the residuals were calculated. Obviously, bacteria (blue squares) had the highest contribution to radioactivity of ^{137}Cs (Figure 12), which showed the strongest correlation with the concentration of ^{137}Cs, followed by the order of little particles (wine squares), spores (violet squares), and ascospores (magenta squares) and fragment (olive squares). It was strongly consistent with the results of the size distribution of particles (as shown in Figure 10c), in which particles with a diameter (< 2 μm) could be the predominant possible carriers of ^{137}Cs. Therefore, combining the information on the size distribution of the particles (Figure 10), the dominant ^{137}Cs-bearing particles could be bacteria (1-1.8 μm), followed with little particles (less than 1 μm) and medium particles of 1.8-10 μm, possibly deriving from spores.

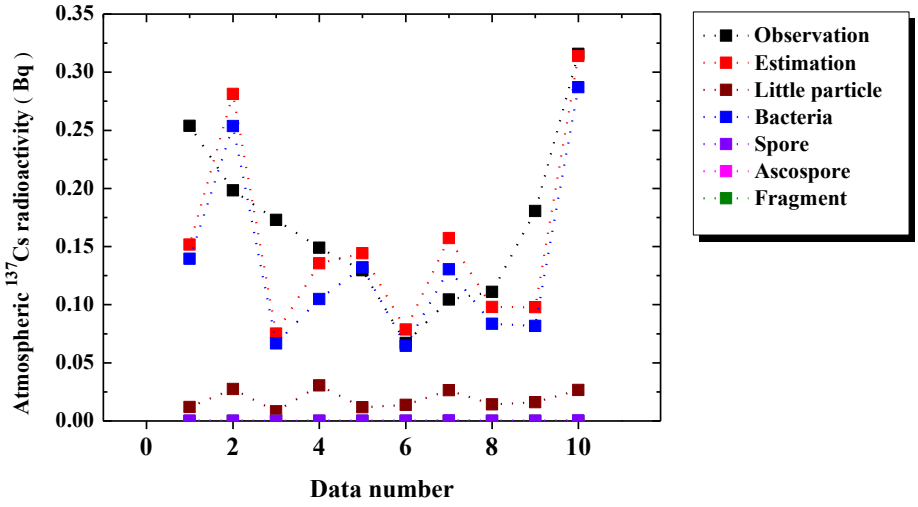

Figure 12. Bioaerosol particles' radioactivity contribution to ^{137}Cs radioactivity based on the multiple linear regression equation (2). The black squares are the measured values (*I*) of ^{137}Cs radioactivity in each HV aerosol filter sample. The red squares represent the estimated values (*I*) from equation (2) in each sample. The rest symbols represent their contributed radioactivity of different bioaerosol particles to the radioactivity of ^{137}Cs based on statistical predictions from the multiple linear regression equation, as

https://doi.org/10.5194/egusphere-2023-2999
Preprint. Discussion started: 15 January 2024

detailed information is summarized in Table 6.

Table 6. Contribution values of each species of bioaerosols to ^{137}Cs radioactivity. There were ten data (for eight in September, two on 15 May, consideration of bioaerosols could be the main carriers). The observed values (Bq) of ^{137}Cs radioactivity are obtained from the HV aerosol filter samples (183.2 mm × 234 mm). The estimated values (Bq) are based on a prediction of equation (2) in each sample. The predicted radioactivity (Bq) in little particles, bacteria, spores, ascospores, and fragments (without considering pollens because of seasonality) was calculated from the statistical analysis in a multiple linear regression equation (2). The residual values were involved in the difference between the measured value and the estimated value.

Data number	Measured value (Bq)	Estimated value (Bq)	Little particle (Bq)	Bacteria (Bq)	Spore (Bq)	Ascospore (Bq)	Fragment (Bq)	Residual value (Bq)
1	0.2538	0.1516	0.0119	0.1395	0.0002	0.0000	0.0000	0.1023
2	0.1983	0.2812	0.0275	0.2536	0.0002	0.0000	0.0000	-0.0829
3	0.1730	0.0751	0.0083	0.0667	0.0001	0.0000	0.0000	0.0980
4	0.1490	0.1355	0.0306	0.1048	0.0002	0.0000	0.0000	0.0134
5	0.1296	0.1442	0.0118	0.1321	0.0003	0.0000	0.0000	-0.0146
6	0.0671	0.0786	0.0139	0.0645	0.0001	0.0000	0.0000	-0.0114
7	0.1045	0.1573	0.0264	0.1305	0.0004	0.0000	0.0000	-0.0528
8	0.1110	0.0980	0.0143	0.0835	0.0002	0.0000	0.0000	0.0130
9	0.1806	0.0978	0.0161	0.0817	0.0001	0.0000	0.0000	0.0828
10	0.3158	0.3139	0.0266	0.2870	0.0004	0.0000	0.0000	0.0019

In addition, to verify the accuracy of equation (2), a correlation analysis between the observed and estimated radioactivity values was shown in Figure 13. The X-axis was the

https://doi.org/10.5194/egusphere-2023-2999
Preprint. Discussion started: 15 January 2024

observed value of the atmospheric radioactivity of ^{137}Cs, and Y-axis was the estimated value of the atmospheric radioactivity of ^{137}Cs. It was obvious that they were in a good positive linear relationship, indicating the feasibility and reasonability of equation (2).

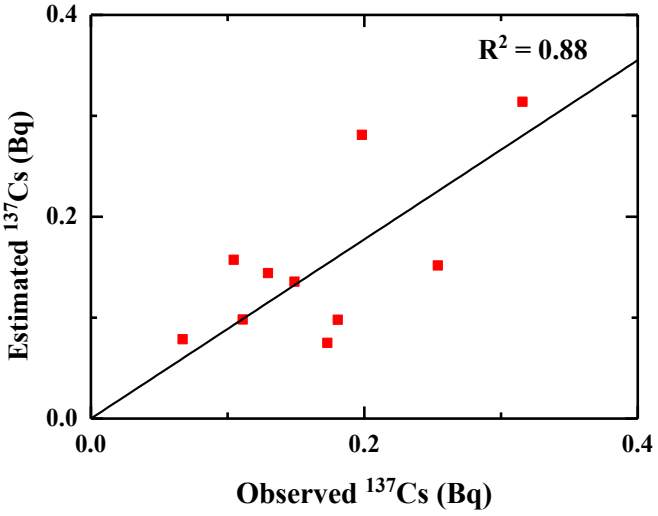

Figure 13. Correlation between observed values and estimated values for ^{137}Cs radioactivity.

4.5 Effect estimation of weather conditions on ^{137}Cs and its carriers

Several representative items of weather conditions, such as precipitation, air temperature, relative humidity, wind speed, and gust wind speed, were selected and monitored to analyze the influence of these weather factors on the concentration of ^{137}Cs and its carriers. Precipitation was obtained from a 12-hour accumulated value, and the other values were the average value, during the sampling period. Table 7 shows the effect of atmospheric ^{137}Cs concentration and concentration of particles in HV aerosol samples by precipitation, air temperature, RH, wind speed, and gust in May 2019, which was estimated by Pearson correlation and P-value significance tests (ten samples were used for analysis, n=10). It could be found that the precipitation had a negative effect on both the concentration of ^{137}Cs and

https://doi.org/10.5194/egusphere-2023-2999
Preprint. Discussion started: 15 January 2024

its carriers. The temperature had a positive effect on the concentration of ^{137}Cs and its carriers, which was consistent with the abovementioned speculation that the concentration of ^{137}Cs was higher in the warm season and lower level in the cold season. Other weather conditions of RH, wind speed, and gust had no significant correlations in the current research.

Table 7. The effect of atmospheric ^{137}Cs and concentration of particles in HV filter samples by precipitation, air temperature, RH, wind speed, and gust in May 2019, was estimated by Pearson correlation and P-value significance tests (ten samples were used for analysis, n=10).

Items	Air ^{137}Cs concentration(Bq m^{-3})		Particle concentration(grain m^{-3})	
	Pearson correlation	P-value	Pearson correlation	P-value
Precipitation(mm)	**-0.38**	0.28	**-0.52**	0.13
Air Temperate(°C)	**0.44**	0.20	**0.48**	0.16
Relative Humidity(%)	-0.16	0.65	-0.07	0.84
Wind Speed(m/s)	0.28	0.43	-0.05	0.90
Gust(m/s)	0.41	0.23	-0.08	0.83

The effect of atmospheric ^{137}Cs and concentration of particles in HV filter samples by precipitation, air temperature, RH, wind speed, and gust in September 2019 was shown in Table 8, also estimating by Pearson correlation and P-value significance tests (eight samples were used for analysis, n=8). Obviously, the temperature had a positive effect on both the concentration of ^{137}Cs and its carriers, which was consistent with the results in May and the speculation. In contrast, the precipitation had a negative impact on the concentration of ^{137}Cs and a positive effect on the concentration of the particles, which was inconsistent with that in May.

In the report (Kita et al., 2020), the precipitation was conducive to an increase of the atmospheric ^{137}Cs compared with the non-rainfall sampling period. In September, the precipitation positively affected the concentration of the bioparticles. Because the rainfall was possible and reasonable to promote spores' multiplication. Moreover, there was no doubt that higher temperature could accelerate microbial colonization, which was able to explain

https://doi.org/10.5194/egusphere-2023-2999
Preprint. Discussion started: 15 January 2024

the positive impact on the concentration of ^{137}Cs and its carriers by temperature both in May and September.

Table 8. The effect of atmospheric ^{137}Cs concentration and concentration of particles in HV filter samples by precipitation, air temperature, RH, wind speed, and gust in September 2019, was estimated by Pearson correlation and P-value significance tests (ten samples were used for analysis, n=8).

Items	Air ^{137}Cs concentration(Bq m^{-3})		Particle concentration(grain m^{-3})	
	Pearson correlation	P-value	Pearson correlation	P-value
Precipitation(mm)	**-0.34**	0.41	**0.34**	0.41
Air Temperate(°C)	**0.27**	0.52	**0.21**	0.63
Relative Humidity(%)	-0.52	0.19	0.06	0.88
Wind Speed(m/s)	-0.17	0.69	-0.26	0.53
Gust(m/s)	-0.15	0.72	-0.29	0.48

5 Conclusions

From the analysis of annual atmospheric concentration variation of ^{137}Cs (based on the HV air filter samples collected in 2019), the atmospheric concentration of ^{137}Cs had a small fluctuation within 0.0002 Bqm^{-3} from January to April and a slightly higher activity level of ^{137}Cs in the air could be observed from May to September. Therefore, it could be obtained that the seasonal variation of ^{137}Cs was higher in the warm season (from May to September) and lower in the cold season (from January to April). Significantly, there were two peaks that appeared in May (about 0.00072 Bqm^{-3}) and September (about 0.00052 Bqm^{-3}). Thus, a lot of attention was given to understanding the difference of concentration variations of ^{137}Cs and its carriers in HV filter samples collected in May and September. By SEM/EDS and optical microscope observations, it could be obtained that the small mineral particles or soil dusts could be the main carriers of ^{137}Cs in early Spring and the carbon-containing particles (some microorganisms, spores, and some other bio-particles) could be the dominated carriers of ^{137}Cs in the late Spring. The bio-particles (bacteria and other small bio-aerosols particles)

https://doi.org/10.5194/egusphere-2023-2999
Preprint. Discussion started: 15 January 2024

could be dominant carriers of ^{137}Cs in September.

According to an effect estimation of atmospheric ^{137}Cs concentration and concentration of particles in HV filter samples by measuring precipitation, air temperature, RH, wind speed, and gust in May and September 2019, using Pearson correlation and P-value significance tests, it could be obtained that the temperature and the precipitation were the main impact factors of ^{137}Cs and its carriers. Specifically, the temperature had a positive effect on the concentration of ^{137}Cs and its carriers both in May and September 2019, which was consistent with the abovementioned speculation that ^{137}Cs concentration was higher in the warm season and lower level in the cold season (Kinase et al., 2018). Moreover, the rainfall had a negative effect on both the concentration of ^{137}Cs and its carriers in May 2019. In contrast, the rainfall had a negative impact on the concentration of ^{137}Cs and a positive effect on the concentration of the particles in 2019, which may be resulted from the fact that the effect of precipitation on the concentration of ^{137}Cs and/or bioparticles may persist for some time. For instance, the rainfall in one day may affect changes of the concentration of ^{137}Cs and/or bioparticles in the following several days. Moreover, there was no decreasing trend in the concentration of ^{137}Cs in 2019, which means long-term monitoring was still necessary for further and deeply understanding the fate and variation of atmospheric ^{137}Cs resuspended from ^{137}Cs bearing microparticles (CsMPs) (Tang et al., 2022; Igarashi et al., 2019a; Higaki et al., 2020; Nihei et al., 2018) or soluble ^{137}Cs (Otosaka et al., 2022) deriving from FDNPP.

Competing interests

The contact author has declared that none of the authors has any competing interests.

References

Christoudias, T. and Lelieveld, J.: Modelling the global atmospheric transport and deposition of radionuclides from the Fukushima Dai-ichi nuclear accident, Atmospheric Chemistry and

https://doi.org/10.5194/egusphere-2023-2999
Preprint. Discussion started: 15 January 2024

Physics, 13, 1425-1438, 2013.

HERP: Ten years after the 2011 off the pacific coast of Tohoku earthquake, 2021.

Higaki, S., Kurihara, Y., and Takahashi, Y.: Discovery of radiocesium-bearing particles in masks worn by members of the public in Fukushima in spring 2013, Health Physics, 118, 656-663, 2020.

Hirose, K.: Temporal variation of monthly 137Cs deposition observed in Japan: effects of the Fukushima Daiichi nuclear power plant accident, Applied Radiation and Isotopes, 81, 325-329, 2013.

Hirose, K.: Atmospheric effects of Fukushima nuclear accident: A review from a sight of atmospheric monitoring, Journal of environmental radioactivity, 218, 106240, 2020.

Hoorman, J. J.: The role of soil bacteria, Ohio State University Extension, Columbus, 1-4, 2011.

IAEA, I.: The Fukushima Daiichi Accident, Report by the Director General,

Igarashi, Y.: Anthropogenic radioactivity in aerosol-a review focusing on studies during the 2000s, Japanese Journal of Health Physics, 44, 313-323, 2009.

Igarashi, Y., Aoyama, M., Hirose, K., Miyao, T., Nemoto, K., Tomita, M., and Fujikawa, T.: Resuspension: decadal monitoring time series of the anthropogenic radioactivity deposition in Japan, Journal of radiation research, 44, 319-328, 2003.

Igarashi, Y., Kogure, T., Kurihara, Y., Miura, H., Okumura, T., Satou, Y., Takahashi, Y., and

https://doi.org/10.5194/egusphere-2023-2999
Preprint. Discussion started: 15 January 2024

Yamaguchi, N.: A review of Cs-bearing microparticles in the environment emitted by the Fukushima Dai-ichi Nuclear Power Plant accident, Journal of environmental radioactivity, 205, 101-118, 2019a.

Igarashi, Y., Kita, K., Maki, T., Kinase, T., Hayashi, N., Hosaka, K., Adachi, K., Kajino, M., Ishizuka, M., and Sekiyama, T. T.: Fungal spore involvement in the resuspension of radiocaesium in summer, Scientific reports, 9, 1954, 2019b.

Ishizuka, M., Mikami, M., Tanaka, T. Y., Igarashi, Y., Kita, K., Yamada, Y., Yoshida, N., Toyoda, S., Satou, Y., and Kinase, T.: Use of a size-resolved 1-D resuspension scheme to evaluate resuspended radioactive material associated with mineral dust particles from the ground surface, Journal of environmental radioactivity, 166, 436-448, 2017.

Kajino, M., Ishizuka, M., Igarashi, Y., Kita, K., Yoshikawa, C., and Inatsu, M.: Long-term assessment of airborne radiocesium after the Fukushima nuclear accident: re-suspension from bare soil and forest ecosystems, Atmos. Chem. Phys., 16, 13149-13172, 10.5194/acp-16-13149-2016, 2016.

Kelly, J. K., Rasch, A., and Kalisz, S.: A method to estimate pollen viability from pollen size variation, American Journal of Botany, 89, 1021-1023, 2002.

Kimura, M.: Seasonal transitions of airborne carriers of radiocesium in spring and early summer: Master's thesis, 2019a.

Kimura, M.: Seasonal transitions of airborne carriers of radiocesium in spring and early

https://doi.org/10.5194/egusphere-2023-2999
Preprint. Discussion started: 15 January 2024

summer, 2019b.

Kinase, T., Kita, K., Igarashi, Y., Adachi, K., Ninomiya, K., Shinohara, A., Okochi, H., Ogata, H., Ishizuka, M., and Toyoda, S.: The seasonal variations of atmospheric 134,137 Cs activity and possible host particles for their resuspension in the contaminated areas of Tsushima and Yamakiya, Fukushima, Japan, Progress in earth and planetary science, 5, 1-17, 2018.

Kita, K., Igarashi, Y., Kinase, T., Hayashi, N., Ishizuka, M., Adachi, K., Koitabashi, M., Sekiyama, T. T., and Onda, Y.: Rain-induced bioecological resuspension of radiocaesium in a polluted forest in Japan, Scientific Reports, 10, 15330, 10.1038/s41598-020-72029-z, 2020.

Maki, T., Hara, K., Yamada, M., Kobayashi, F., Hasegawa, H., and Iwasaka, Y.: Epifluorescent microscopic observation of aerosol, Earozoru Kenkyu, 28, 201-207, 2013.

MEXT: Aircraft monitoring by surveying the distribution of radioactive materials by MEXT (converted on March 11, 2013), 2013.

Nihei, N., Yoshimura, K., Okumura, T., Tanoi, K., Iijima, K., Kogure, T., and Nakanishi, T.: Secondary radiocesium contamination of agricultural products by resuspended matter, Journal of Radioanalytical and Nuclear Chemistry, 318, 341-346, 2018.

Ohara, T., Morino, Y., and Tanaka, A.: Atmospheric behavior of radioactive materials from Fukushima Daiichi nuclear power plant, Hoken Iryo Kagaku, 60, 292-299, 2011.

Onda, Y., Taniguchi, K., Yoshimura, K., Kato, H., Takahashi, J., Wakiyama, Y., Coppin, F., and Smith, H.: Radionuclides from the Fukushima Daiichi nuclear power plant in terrestrial

https://doi.org/10.5194/egusphere-2023-2999
Preprint. Discussion started: 15 January 2024

systems, Nature Reviews Earth & Environment, 1, 644-660, 2020.

Otosaka, S., Kamidaira, Y., Ikenoue, T., and Kawamura, H.: Distribution, dynamics, and fate of radiocesium derived from FDNPP accident in the ocean, Journal of Nuclear Science and Technology, 59, 409-423, 2022.

Sato, I., Sasaki, J., Satoh, H., Deguchi, Y., Otani, K., and Okada, K.: Distribution of radioactive cesium and its seasonal variations in cattle living in the" difficult - to - return zone" of the Fukushima nuclear accident, Animal Science Journal, 87, 607-611, 2016.

Stanley, R. G. and Linskens, H. F.: Pollen: biology biochemistry management, Springer Science & Business Media2012.

Steinhauser, G., Niisoe, T., Harada, K. H., Shozugawa, K., Schneider, S., Synal, H.-A., Walther, C., Christl, M., Nanba, K., and Ishikawa, H.: Post-accident sporadic releases of airborne radionuclides from the Fukushima Daiichi nuclear power plant site, Environmental science & technology, 49, 14028-14035, 2015.

Tang, P., Kita, K., Igarashi, Y., Satou, Y., Hatanaka, K., Adachi, K., Kinase, T., Ninomiya, K., and Shinohara, A.: Atmospheric resuspension of insoluble radioactive cesium-bearing particles found in the difficult-to-return area in Fukushima, Progress in Earth and Planetary Science, 9, 17, 2022.

TEPCO: The record of the earthquake intensity observed at Fukushima Daiichi Nuclear Power Station and Fukushima Daini Nuclear Power Station (Interim Report), 2011a.

https://doi.org/10.5194/egusphere-2023-2999
Preprint. Discussion started: 15 January 2024

TEPCO: Plant status of Fukushima Daiichi Nuclear Power Station (as of 0 AM March 12th), 2011b.

Yamamoto, N., Bibby, K., Qian, J., Hospodsky, D., Rismani-Yazdi, H., Nazaroff, W. W., and Peccia, J.: Particle-size distributions and seasonal diversity of allergenic and pathogenic fungi in outdoor air, The ISME journal, 6, 1801-1811, 2012.